**Showcasing research from the Department of Materials Science and Nanotechnology Engineering, Abdullah Gül University, Turkey and the Scientific and Technological Research Council of Turkey-Marmara Research Center.**

A hybridized local and charge transfer excited state for solution-processed non-doped green electroluminescence based on oligo(*p*-phenyleneethynylene)

A novel highly efficient green emissive oligo(*p*-phenyleneethynylene)-based hot-exciton molecule is reported with very high photoluminescence (PL) quantum efficiency and strong dipole-dependent excitonic behavior covering the full visible spectrum. The solid-state solvation effect in OLED devices yields HLCT electronic behavior yielding very favorable reverse intersystem crossings (RISCs). Delayed fluorescence due to RISC was evident in the PL decay lifetime measurements with a ns-scale lifetime of ~10 ns.
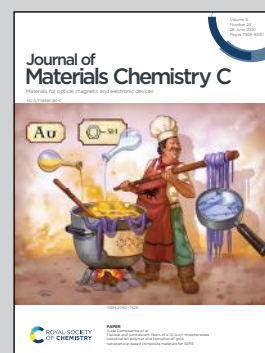
ROYAL SOCIETY
OF **CHEMISTRY**

rsc.li/materials-c

PAPER

Check for updates

A hybridized local and charge transfer excited state for solution-processed non-doped green electroluminescence based on oligo(*p*-phenyleneethynylene)†

Hakan Usta, [ID] *[a] Dilek Alimli, [ID] [b] Resul Ozdemir, [ID] [a] Emine Tekin,[c] Fahri Alkan,[a] Rifat Kacar,[c] Ahu Galen Altas, [ID] [c] Salih Dabak,[c] Ayşe Gül Gürek, [ID] [b] Evren Mutlugun, [ID] [d] Ahmet Faruk Yazici[a] and Ayse Can[a]

We herein report a new highly efficient green emissive hot-exciton molecule, 1,4-bis((4′-diphenylamino-3-cyano-[1,1′-biphenyl]-4-yl)ethynyl)-2,5-bis(2-ethylhexyloxy)benzene (**2EHO-TPA-CNPE**) that consists of an extended D′−π′−A−π−D−π−A−π′−D′ molecular π-system with diphenylamino end units (D′) and ethynylene/phenylene spacers (π/π′). The new molecule exhibits high photoluminescence (PL) quantum efficiencies (Φ_{PL} = 0.95 (solution) and 0.45 (spin-coated neat thin-film)), and a strong PL solvatochromic behavior revealing significant changes in excited state energies/characteristics (locally excited (LE) → hybridized local and charge transfer (HLCT) → charge-transfer (CT)) depending on solvent polarity. Highly efficient (radiative exciton yield (η_r) = 50−59% ≫ 25%) green-emitting OLEDs were fabricated in a conventional device architecture by employing (non-)doped thin-films reaching a maximum current efficiency (CE_{max}) of 12.0 cd A^{-1} and a maximum external quantum efficiency (EQE_{max}) of 5.5%. The emission profile of the non-doped OLED has CIE 1976 (*u′, v′*) chromaticity coordinates of (0.10, 0.55) corresponding to a night vision imaging system (NVIS) compatible Green A region. **2EHO-TPA-CNPE**-based OLED devices of industrial relevance were also fabricated by ink-jet printing the emissive layer and by fabricating an inverted architecture, which possessed respectable device performances of 2.4−6.1 cd A^{-1}. The solid-state solvation effect in OLED devices yields HLCT electronic behavior resulting in high η_r's, which is confirmed by TDDFT to originate from energetically/spatially favorable reverse intersystem crossings (RISCs) (T$_{2/3}$ → S$_1$). As a unique observation, delayed fluorescence due to this RISC was evident in the PL decay lifetime measurement with a ns-scale lifetime of ∼10 ns. These results clearly allow a better understanding of the structure–photophysical property–electroluminescence relationships in this new class of oligo(*p*-phenyleneethynylene)-based hot-exciton molecules, and it could open up new opportunities for high-performance solution-processed optoelectronic/sensing applications.

Introduction

The development of rare-metal-free emissive materials in organic light-emitting diode (OLED) applications for flat-panel displays and solid-state lightings has greatly focused on fluorescent small molecules, which offers all the intrinsic advantages (*i.e.*, well-defined structure, high purity, expensive metal-free, low-cost, good solubility, and synthetic reproducibility) of molecular

[a] *Department of Materials Science and Nanotechnology Engineering, Abdullah Gül University, 38080 Kayseri, Turkey. E-mail: hakan.usta@agu.edu.tr*

[b] *Department of Chemistry, Gebze Technical University, 41400 Gebze, Kocaeli, Turkey*

[c] *The Scientific and Technological Research Council of Turkey (TUBITAK)-Marmara Research Center (MAM), 41470 Gebze, Kocaeli, Turkey*

[d] *Department of Electrical and Electronics Engineering, Abdullah Gül University, 38080 Kayseri, Turkey*

† Electronic supplementary information (ESI) available: Calculated UV-Vis absorption spectrum of **2EHO-TPA-CNPE** and the molecular orbitals involved in the low-lying excited states (Fig. S1); synthesis of **2EHO-DEB** (Scheme S1); chemical characterizations (^{1}H NMR for intermediate compounds 1, 2, and **2EHO-DEB** (Fig. S2–S4), and ^{1}H/^{13}C NMR and MALDI TOF-MS spectra for **2EHO-Br-CNPE** and **2EHO-TPA-CNPE** (Fig. S5–S10)); solvatochromic optical absorption/photoluminescence spectra of **2EHO-TPA-CNPE** in different solvents (Fig. S11 and S12); solvatochromic Lippert–Mataga model for deep-blue emissive **2EHO-CNPE** (Fig. S13); atomic force microscopy (AFM) image of spin-coated **2EHO-TPA-CNPE** thin-film (Fig. S14); photoluminescence/electroluminescence spectra of doped OLED device (Fig. S15); luminance–voltage–current density and current efficiency–current density–external quantum efficiency for the doped, inverted, and ink-jet printed OLED devices (Fig. S16–S18); natural transition orbitals of the S$_4$ and T$_8$ states (Fig. S19); theoretical excited state data and matrix elements for the coupling between singlet and triplet states (Tables S3 and S4). See DOI: 10.1039/d0tc01266a

This journal is © The Royal Society of Chemistry 2020

J. Mater. Chem. C, 2020, **8**, 8047–8060 | 8047

materials for use in new generation optoelectronics.[1–8] In particular, fluorescent small molecules having proper molecular sizes and solution rheological properties could be printed into pixelated emissive layers, which is of critical importance for future solution processed and printed optoelectronic technologies.[9–11] However, as controlled by spin statistics of electrically generated excitons and spin-allowed electronic transitions,[12] conventional fluorescent small molecules generally suffer from a limited emission efficiency (radiative exciton yields ($\eta_{\text{r-max}}$) = 25%) during electroluminescence, which makes them less attractive as compared to their inorganic and phosphorescent counterparts.[13,14] Since only the singlet excited state of a molecule could decay radiatively to the singlet ground state, developing properly designed unconventional molecular π-systems that could increase singlet excited state population through triplet-to-singlet excited state conversions is particularly important.[1] This has become an attractive avenue in recent years to achieving high ($\gg 25\%$) η_{r}'s. In this regard, much progress has been made in triplet–triplet annihilation (TTA) and thermally activated delayed-fluorescence (TADF) approaches.[15,16] In these systems, while TTA generates an extra singlet exciton through fusion of two T_1 excitons intrinsically limiting $\eta_{\text{r-max}}$ to 62.5%,[17] TADF is based on thermal energy assisted reverse intersystem crossing (RISC) of T_1 excitons to energetically close (typically within ~ 0.1–0.3 eV) S_1 excitons yielding very high $\eta_{\text{r-max}}$'s of more than ~ 80–90%.[18] Although both mechanisms enhance the overall electroluminescence performance in fluorescent OLEDs, accumulation of relatively long-lived T_1 excitons could cause serious efficiency roll-off at high current densities owing to undesired triplet–triplet

annihilation and singlet–triplet quenchings.[19,20] Activation of hot-exciton RISC channels in the upper excited states (T_n ($n > 1$) → S_m ($m \geq 1$)), which is as an exception to the classic Kasha's rule in photochemistry,[21] has recently been unveiled as an effective third approach (Fig. 1A). When the proper electronic conditions are met, RISC occurring from high-lying T_n to S_m was shown to be fast process (several nanoseconds)[22] and could compete with the internal conversions down to T_1 state.[23] From an energy-gap-law standpoint, for hot-exciton channels to operate with a fast RISC rate, the energy of the high-lying triplet state should be close to that of the corresponding singlet excited state and far from T_1 to deactivate low-lying triplet internal conversions ($\Delta E_{S_m\text{-}T_n} \ll \Delta E_{T_n\text{-}T_1}$ for $k_{\text{RISC}} \gg k_{\text{IC(T)}}$). For triplet and singlet excited states involved in the hot-exciton channels, the configurations of the natural transition orbitals (NTOs) should possess both locally excited (LE) and charge-transfer (CT) characteristics, namely hybridized local and charge transfer (HLCT) excited state (Fig. 1A). In a HLCT excited state, while LE character enables highly efficient fluorescence emission (large transition moment) arising from large wave function overlap, CT character decreases the binding energies of spatially separated excitons yielding small energetic splitting (quasidegenerate singlet and triplet excitons) and facilitates triplet-to-singlet excitonic transitions.[24–27] Combining both characteristics into a single HLCT excited state form is key to developing highly emissive fluorescent molecules with high singlet exciton generation ($\eta_{\text{r}} \gg 25\%$).[28]

In the past decade, a number of molecules with HLCT and hot-exciton properties in OLED devices have been developed following the first report (**TPA-PPI** in Fig. 1B) by Ma et al. in
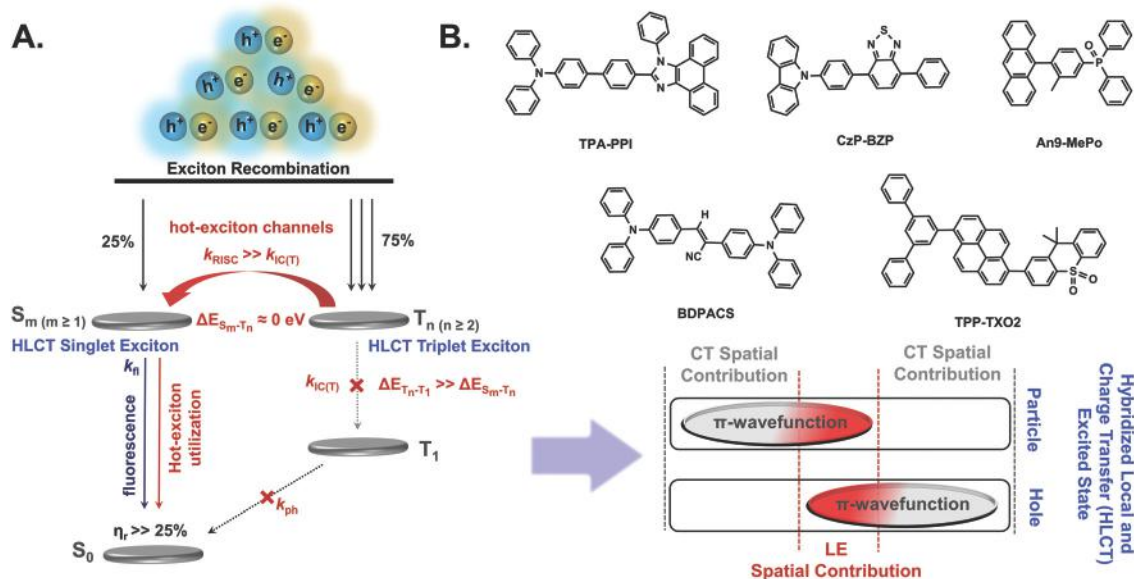

Fig. 1 (A) The schematic of exciton recombination and radiative decay through hot-exciton mechanism in an electroluminescence process indicating energy levels of molecular electronic states and energetic/wave function requirements (k_{RISC}, reverse intersystem crossing rate; $k_{\text{IC(T)}}$, triplet internal conversion rate; $k_{\text{ph}}/k_{\text{fl}}$, phosphorescence/fluorescence rate; η_{r}, radiative exciton yield). (Note that if $m > 1$ ($n > 2$) additional internal conversions among singlet (triplet) states would occur). The illustration of hybridized local and charge transfer (HLCT) excited state formation on a molecular π-backbone with regards to hole/particle natural transition orbitals indicating locally excited (LE) and charge transfer (CT) spatial contributions. (B) Chemical structures of HLCT hot-exciton small molecules reported in the literature with values of $\eta_{\text{r}} \gg 25\%$ in the OLEDs.[19,29–32]

2012 (see Table S1, ESI† for the full list).[19,29–32] The general molecular design strategy involves constructing π-systems with donor (D) and acceptor (A) moieties to yield extended π-delocalization (LE character) with controlled Frontier orbital wave function separation (CT character) for efficient charge-transport, radiative electronic transition, and large singlet exciton generation. To this end, π-electron rich structures such as triphenylamine,[24,32–34] carbazole,[29] anthracene,[19] pheno-thiazine,[35] tetraphenylethene,[36] and pyrene[31] have been employed as donor units; π-electron deficient structures such as phenanthro[9,10-d]imidazole,[32,34] naphtho[2,3-c][1,2,5]thiadia-zole,[24] triphenylphosphine oxide,[19] benzothiadiazole,[29,35] and thioxanthene-S,S-dioxide[31] have been used as acceptor units (Fig. 1B and Table S1, ESI†). In these HLCT molecules, the hybridization of LE and CT is engineered by employing a number of design approaches such as tuning D–A interring twists and intramolecular π-conjugation length,[19,28] introdu-cing π-spacer between D and A units,[37] and changing the electronic strength of D and A units.[29,34] To this end, we have recently demonstrated for the first time that D–A functionalized oligo(p-phenyleneethynylene) π-framework offers an ideal elec-tronic structure and optical properties to form HLCT excited states and hot-exciton channels for high radiative exciton yields ($\eta_r \sim 70\% \gg 25\%$) in OLEDs.[38] Record high external quantum efficiency (EQE) of ~7.1% has been achieved with our previously developed 1,4-bis((2-cyanophenyl)ethynyl)-2,5-bis(2-ethylhexyloxy)-benzene (2EHO-CNPE, Fig. 2) in solution-processed deep-blue (Commission Internationale de l'Eclairage CIE(x, y) = 0.15, 0.09) emitting OLEDs. Ethynylene (–C≡C–) π-spacers have played a critical role in this π-system between D and A units to yield HLCT excited state properties and very effective hot exciton channels ($T_3/T_2 \rightarrow S_1$) ($\Delta E_{T_3/T_2-S_1} = 0.01–0.08$ eV $\ll \Delta E_{T_2-T_1} = 0.81$ eV). Motivated with these promising results, we envision to visit further π-extended oligo(p-phenyleneethynylene) π-systems with the goal of realizing color coordinates in lower energy regions (i.e., green in this study) and elucidating the formation

of hot-exciton channels/HLCT characteristics. With regards to designing efficient fluorescent molecules with a wide-color-gamut for high performance display and lighting applications, it is still of utmost urgency to study and expand the library of π-extended HLCTs, especially considering that the majority of hot-exciton molecules are high energy (deep-blue/blue) emissive π-systems (Table S1, ESI†). Going from high energy deep-blue to lower energy emissive systems, energetic separa-tions and HLCT characteristics of π-electronic states might greatly change.[19,28]

Herein, we report the design, synthesis, and full charac-terization of a new rod-shaped oligo(p-phenyleneethynylene) molecule, 1,4-bis((4′-diphenylamino-3-cyano-[1,1′-biphenyl]-4-yl)ethynyl)-2,5-bis(2-ethylhexyloxy)benzene (2EHO-TPA-CNPE, Fig. 2). In this new molecular π-system, an extended D′–π′–A–π–D–π–A–π′–D′ molecular architecture with diphenylamino end units (D′) and ethynylene/phenylene π-spacers (π/π′) was employed to achieve highly efficient green luminescence. The thermal, photophysical, electrochemical, and electroluemines-cence device characteristics of the new molecule have been studied in detail. High photoluminescence quantum efficiencies (Φ_{PL}'s) of 0.95 and 0.45 were measured (λ_{fl}^{max} at 518–519 nm) in solution and as spin-coated neat thin-film, respectively, by using integrating-sphere. Solvent-dependent photoluminescence study revealed a strong solvatochromic behavior for the new molecule showing significant changes in the excited state energies ($\Delta\lambda_{fl}^{max} = +130$ nm) and characteristics (LE → HLCT → CT) upon polarity increase. Similar polarity effect was also evident in the electro-luminescence of the emissive thin-film in OLEDs that solid-state solvation effect tunes emission profile and radiative exciton yield. The (non-)doped emissive thin-films were found to be in a medium polarity environment to facilitate HLCT characteristics. Highly efficient ($\eta_r = 50\% \gg 25\%$) green-emitting OLEDs were fabricated in a conventional device architecture by employing spin-coated non-doped emissive 2EHO-TPA-CNPE thin-film, which showed maximum current efficiency (CE_max)
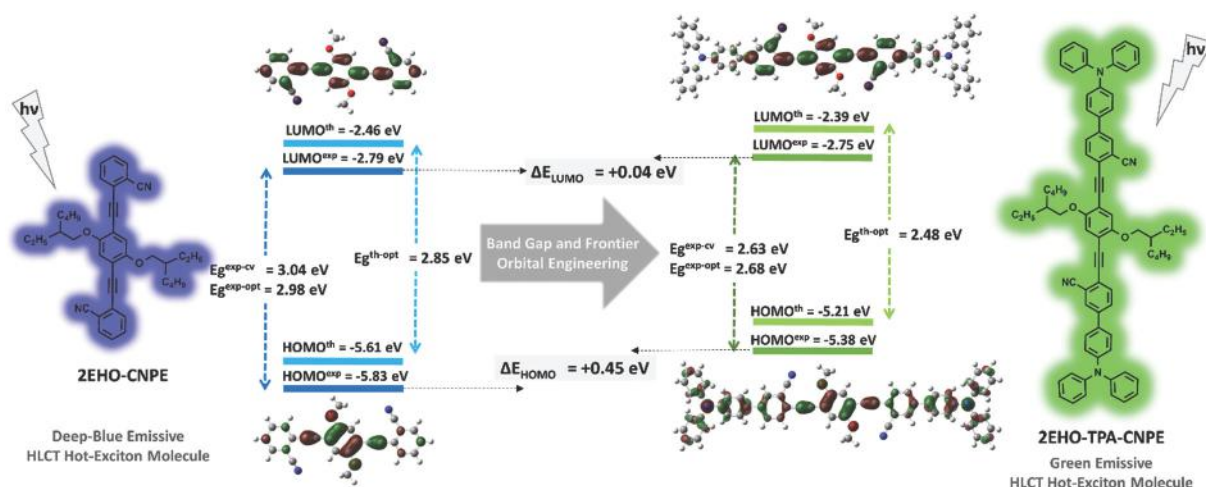

Fig. 2 The chemical structures of deep-blue emissive molecule 2EHO-CNPE developed in our earlier study[38] and green emissive molecule 2EHO-TPA-CNPE developed in this study, and the energy diagrams showing theoretically calculated (light colors) and experimentally estimated (dark colors) HOMO/LUMO energy levels, Frontier orbital topographies, and optical/electrochemical/theoretical band gaps.

of 12.0 cd A^{-1}, a maximum power efficiency (PE_{max}) of 5.4 lm W^{-1}, and a maximum external quantum efficiency (EQE_{max}) of 4.5%. The emission profile of the non-doped OLED has CIE 1976 (u', v') chromaticity coordinate of (0.10, 0.55) corresponding to a night vision imaging systems (NVIS) compatible Green A region. Additional OLEDs were fabricated by doping the new molecule in CBP host matrix, which exhibits a sky-blue emission with improved EQE_{max} of 5.5% (η_r = 59% $\gg$ 25%). **2EHO-TPA-CNPE**-based OLED devices of industrial relevance were also fabricated by ink-jet printing the emissive layer and by fabricating an inverted architecture, which showed respectable device performances of 2.4 cd A^{-1} and 6.1 cd A^{-1}, respectively. TDDFT calculations reveal that the observed high radiative exciton yield originates from very effective RISC processes between energetically/spatially suitable HLCT excited states ($T_{2/3} \rightarrow S_1$). A ns-scale delayed fluorescence ($\sim$10 ns) due to high-lying (R)ISCs was confirmed in the PL decay profile following a prompt fluorescence decay ($\sim$1 ns). To the best of our knowledge, this result is one of the very few examples in the hot-exciton literature that high-lying RISC-related delayed fluorescence is directly observed in a PL decay profile without using a triplet sensitizer.

Experimental section

Materials and methods

Unless otherwise noted, all reagents were purchased from commercial sources and used as received. Schlenk techniques were employed and all the reactions were carried out under N_2 atmosphere. ^{1}H/^{13}C NMR spectra were recorded using a Bruker 400 spectrometer (for ^{1}H: 400 MHz and for ^{13}C: 100 MHz). Elemental analyses were done using a LecoTruspec Micro model instrument. MALDI-TOF characterization was performed on a Bruker Microflex LT MALDI-TOF-MS Instrument. Thermal characterizations including thermogravimetric analysis (TGA) and differential scanning calorimetry (DSC) measurements were performed under nitrogen at a heating rate of 10 $°C$ min^{-1} using Mettler Toledo-TGA/STDA 851 and Mettler Toledo-DSC 822 model instruments, respectively. UV-Vis absorption spectra were recorded on a Shimadzu, UV-1800 UV-Vis spectrophotometer. Photoluminescence (PL) characterizations were carried out with Agilent-Cary Eclipse fluorescence spectrophotometer. Time-correlated single photon counting measurements were performed using Pico Quant FluoTime 200 equipped with 375 nm pulsed laser diode. The PL quantum yields in solution and solid state were measured (λ_{exc} = 350 nm) on a Hamamatsu absolute PL Quantum Yield Spectrometer C11347 using the integrating-sphere method. Electrochemical measurements were carried out on a BAS-Epsilon potentiostat/galvanostat from Bioanalytical Systems Inc. (Lafayette, IN) equipped with a C3-cell stand. Theoretical calculations except for the ones involving spin–orbit couplings were performed by Gaussian 09 using density functional theory (DFT) and time-dependent density functional theory (TDDFT) at the B3LYP/6-311G** level.[39] For spin–orbit couplings between singlet and triplet states,

we employed the perturbative approach of zeroth-order regular approximation (ZORA) Hamiltonian with B3LYP/TZP level of theory as implemented in ADF2019 program package.[40–42]

Synthesis and structural characterization

Synthesis of 1,4-bis((4-bromo-2-cyanophenyl)ethynyl)-2,5-bis(2-ethylhexyloxy)benzene (2EHO-Br-CNPE). The reagents 5-bromo-2-iodobenzonitrile (0.507 g, 1.646 mmol), CuI (0.007 g, 0.036 mmol), and Pd(PPh$_3$)$_2$Cl$_2$ (0.048 g, 0.068 mmol) in Et$_3$N : THF (2 : 1) (15 mL) were stirred for 5 minutes. Then, 1,4-bis-(ethynyl)-2,5-bis(2-ethylhexyloxy)benzene (**2EHO-DEB**) (0.263 g, 0.687 mmol) in 3 mL of THF was added, and the resulting reaction mixture was heated at 80 $°C$ under nitrogen for 24 h. The solution was cooled down to room temperature and evaporated to dryness to yield a crude compound. The crude product was then purified by column chromatography on silica gel using dichloromethane : n-hexane (3 : 2) solvent mixture to afford **2EHO-Br-CNPE** as a pure light yellow solid (0.362 g, 71% yield). ^{1}H NMR (400 MHz, CDCl$_3$): δ 7.82 (d, 2H, J = 4.0 Hz), 7.72 (d, 1H, J = 4.0 Hz), 7.70 (d, 1H, J = 4.0 Hz), 7.49 (s, 1H), 7.47 (s, 1H), 7.08 (s, 2H), 3.93–3.95 (m, 4H), 1.79–1.85 (m, 2H), 1.54–1.59 (m, 8H), 1.27–1.37 (m, 8H), 0.95 (t, 6H, J = 12.0 Hz), 0.87 (t, 6H, J = 16.0 Hz). ^{13}C NMR (100 MHz, CDCl$_3$): δ 154.1, 135.7, 135.3, 133.5, 126.3, 121.9, 116.6, 116.4, 116.2, 113.6, 93.9, 90.3, 72.3, 38.0, 31.9, 30.1, 29.7, 26.9, 22.7, 14.1. $T_{m.p.}$ = 68–69 $°C$. MS(MALDI-TOF) m/z (M$^+$): calcd for C$_{40}$H$_{42}$Br$_2$N$_2$O$_2$: 740.16, found: 515.987 for [M-2 $\times$ (2EH)]$^+$, 438.772 for [M-2 $\times$ (2EH)-Br]$^+$. Anal. calcd for C$_{40}$H$_{42}$Br$_2$N$_2$O$_2$: C, 64.70; H, 5.70; N, 3.77; found: C, 64.38; H, 5.99; N, 3.44.

Synthesis of 1,4-bis((4′-diphenylamino-3-cyano-[1,1′-biphenyl]-4-yl)ethynyl)-2,5-bis(2-ethylhexyloxy)benzene (2EHO-TPA-CNPE). The solution of 1,4-bis((4-bromo-2-cyanophenyl)ethynyl)-2,5-bis-(2-ethylhexyloxy)benzene (**2EHO-Br-CNPE**) (0.315 g, 0.424 mmol) and 4-(diphenylamino)phenylboronic acid pinacol ester (0.347 g, 0.935 mmol) in 20 mL of dimethoxyethane (DME) was stirred at room temperature for 5 min. Then, Pd(PPh$_3$)$_4$ (0.024 g, 0.021 mmol) and Na$_2$CO$_3$ (0.395 g, 3.73 mmol) in 5 mL of water were added, and the resulting mixture was heated at 80 $°C$ under nitrogen for 24 h. After the reaction was completed, the mixture was cooled down to room temperature and quenched with water. The reaction mixture was then extracted with chloroform, and the organic phase was washed with water, dried over Na$_2$SO$_4$, filtered, and evaporated to dryness to give a crude product. The crude product was then purified by column chromatography on silica gel using dichloromethane : n-hexane (3 : 1) solvent mixture to afford **2EHO-TPA-CNPE** as a pure yellow solid (0.295 g, 65% yield). ^{1}H NMR (400 MHz, CDCl$_3$): δ 7.88 (s, 2H), 7.75 (d, 2H, J = 8.0 Hz), 7.64 (d, 2H, J = 8.0 Hz), 7.45 (d, 4H, J = 8.0 Hz), 7.33 (s, 2H), 7.29 (d, 8H, J = 8.0 Hz), 7.07–7.17 (m, 16H), 3.95 (t, 4H, J = 8.0 Hz), 1.83–1.86 (m, 2H), 1.54–1.59 (m, 8H), 1.26–1.35 (m, 8H), 0.96 (t, 6H, J = 16.0 Hz), 0.87 (t, 6H, J = 16.0 Hz). ^{13}C NMR (100 MHz, CDCl$_3$): δ 154.1, 148.5, 147.3, 140.8, 132.8, 131.3, 130.5, 130.1, 129.5, 127.6, 124.9, 123.6, 123.1, 117.8, 116.7, 115.3, 113.7, 93.0, 91.3, 72.0, 39.5, 30.6, 29.1, 24.0, 23.1, 14.1, 11.3. $T_{m.p.}$ = 193–194 $°C$. MS(MALDI-TOF) m/z (M$^+$): calcd for C$_{76}$H$_{70}$N$_4$O$_2$: 1070.55,

8050 | *J. Mater. Chem. C*, 2020, **8**, 8047–8060

This journal is © The Royal Society of Chemistry 2020

found: 1071.698 for $[M + H]^+$. Anal. calcd for $C_{76}H_{70}N_4O_2$: C, 85.20; H, 6.59; N, 5.23; found: C, 85.37; H, 6.39; N, 5.41.

OLED device fabrication and characterization

The green light-emitting diode devices studied here were fabricated based on the architecture of ITO/PEDOT:PSS(60 nm)/**2EHO-TPA-CNPE**(55 nm)/TPBI(40 nm)/LiF(0.8 nm)/Al(100 nm) for conventional devices and ITO/TNC(50 nm)/**2EHO-TPA-CNPE**(55 nm)/TPD(50 nm)/V$_2$O$_5$(15 nm)/Al(100 nm) for inverted devices. First, patterned indium tin oxide (ITO) (10 Ω square^{-1}, 120 nm, Kintec Company) substrates were cleaned with distilled water, and acetone–ethanol–isopropanol in an ultrasonic solvent bath, and then treated by oxygen plasma for 5 min. For the conventional device, poly(3,4-ethylenedioxythiophene):poly-(styrenesulfonate) (PEDOT:PSS, Heraeus Clevios GmbH) was spin-coated (3000 rpm for 60 s) on cleaned ITO-glass substrates as the hole-injecting layer (60 nm) and baked at 120 °C for 20 min. 10 mg of **2EHO-TPA-CNPE** solid was dissolved in 1 mL of chloroform and filtered through a filter (0.20 μm, Millipore, PTFE). Then, **2EHO-TPA-CNPE** solution was spin-coated on PEDOT:PSS at a speed of 1500 rpm (40 s) and annealed at 80 °C for 10 min to remove residual solvent, which afforded the green emissive layer (55 nm). For ink-jet-printed devices, **2EHO-TPA-CNPE** thin-film (50 nm) was printed from the ink formulation (1 mg ml^{-1}) prepared in o-xylene:phenoxytoluene solvent mixture (50:50 v/v%). Then, electron-transport/hole-blocking 1,3,5-tris-(phenyl-2-benzimidazolyl)benzene (TPBI) layer was deposited by thermal evaporation at a pressure of 2×10^{-6} Pa. The thickness of the TPBI layer was 40 nm. Finally, a cathode composed of LiF (0.8 nm) and aluminum (100 nm) were sequentially deposited via thermal evaporation under high vacuum (2×10^{-6} Pa). For inverted OLEDs, ZnO:PEI:TPBi ternary nano-composite (TNC) was prepared as specified.[43] TNC solution was spin coated at 2500 rpm for 30 seconds on cleaned ITO glass substrates and cured at 120 °C for 120 minutes in ambient air to give the electron-injecting layer (50 nm). Then, **2EHO-TPA-CNPE** solution was spin-coated on the TNC layer (1500 rpm 40 s) and annealed at 80 °C for 10 min. Next, TPD (N,N'-bis(3-methylphenyl)-N,N'-diphenylbenzidine) (50 nm) was deposited as the hole transport layer by thermal evaporation at a pressure of 2×10^{-6} Pa. V$_2$O$_5$ (15 nm) and aluminum (100 nm) were evaporated as the hole-injecting layer and the cathode, respectively. The size of the active OLED area is 9 mm^2. The electroluminescence spectra and current density–voltage–brightness of the devices were measured by Hamamatsu PMA-12 C10027 Photonic Multichannel analyzer. The thicknesses of the organic layers were measured by a stylus profiler (KLA Tencor P-6). The surface morphology of the emissive **2EHO-TPA-CNPE** thin-film spin-coated on ITO/PEDOT:PSS was characterized by atomic force microscopy (FlexAFM-NanoSurf, Abdullah Gül University-Central Research Facility (AGU-CRF)).
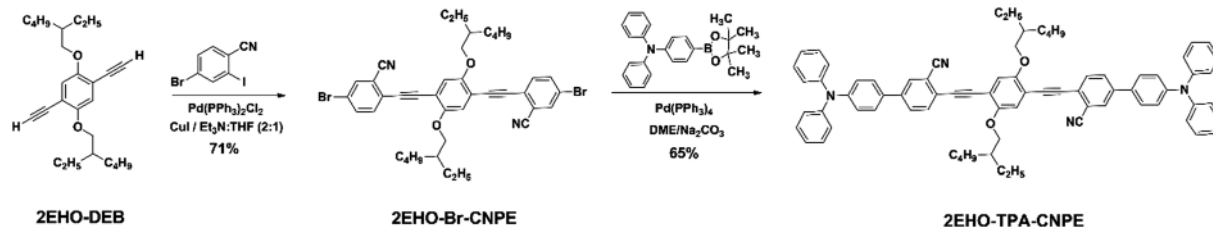
Results and discussion

Molecular design, synthesis, and characterization

The D'–π'–A–π–D–π–A–π'–D' molecular architecture of **2EHO-TPA-CNPE** with diphenylamino end units (D') and

ethynylene/phenylene π-spacers (π/π') is envisioned to give an extended π-system for green emission, facilitate hole injection/transport characteristics of the emissive layer,[44] and improve thermal/morphological stability of the deposited films. The presence of highly twisted aryl substituents at molecular termini and swallow-tailed substituents is expected to allow for good solubility and impede undesired aggregation and intermolecular interactions in the solid-state (i.e., reduced excimer formation/non-radiative decays), which might enable the solution-based fabrication of non-doped emissive layer (i.e., no host matrix).[45] Considering the good solubility and the decent molecular size (1071.39 amu) (i.e., potentially good solution rheology), fabrication of an emissive layer based on the new molecule could be achieved even by using printing techniques such as ink-jet printing. Ethynylene and phenylene π-spacers are employed between D and A units to control the optical band gap, and facilitate efficient fluorescence emission by adjusting the formation of LE character in the HLCT excited states. It's noteworthy that, different than our initial design,[38] the presence of additional π-electron rich D end units in the new molecule is very likely to enhance the CT characteristics of the HLCT excited states. Finally, the coexistence of donor and acceptor π-units in the same molecular backbone could allow for ambipolar charge-transport, which is crucial for efficient electroluminescence in organic thin-films.[46]

The quantum mechanical modelling (DFT, B3LYP/6-311G**) shows that the theoretical HOMO and LUMO energies of the new molecule are −5.21 eV and −2.39 eV, respectively, which indicates a very similar LUMO and a significantly increased HOMO (ΔE_{HOMO} = +0.45 eV) as compared to the deep blue emissive **2EHO-CNPE** (Fig. 2). The calculated absorption spectrum shows that S$_0 \to$ S$_1$ (HOMO $\to$ LUMO; f = 2.32) electronic transition occurs at 2.48 eV ($\sim$500 nm), which is very likely to produce green molecular emission (Fig. S1, ESI†). The HOMO of the new molecule is found to be delocalized along the entire molecular π-system signifying the strong donor effect of the diphenylamino termini, which is expected to benefit hole-injection/transport in the new emissive thin-film. On the other hand, LUMO tends to delocalize on the central A–π–D–π–A part giving a LUMO topography that is almost identical to that of **2EHO-CNPE**. This explains the minimal change in the LUMO energy level going from **2EHO-CNPE** to **2EHO-TPA-CNPE**, which is expected to retain a good electron injection/transport character in the new emissive thin-film. Based on Frontier orbital topographies of the new molecule, it is reasonable to suggest that both LE and CT characteristics would be utilized during electronic transitions that could yield an efficient green electroluminescence with favorable emission characteristics. These initial theoretical outcomes are found to be in good agreement with the experimental characterizations (vide infra).

Scheme 1 shows the synthesis route for the new green emitter **2EHO-TPA-CNPE**, which involves two successive Pd-catalyzed cross-coupling reactions starting from **2EHO-DEB** that was synthesized following our previously described procedure (Scheme S1, ESI†). **2EHO-DEB** was first reacted with 5-bromo-2-iodobenzonitrile in the presence of Pd(PPh$_3$)$_2$Cl$_2$ catalyst and

This journal is © The Royal Society of Chemistry 2020

J. Mater. Chem. C, 2020, 8, 8047–8060 | 8051

Scheme 1 The synthesis route for green emissive molecule 1,4-bis((4′-diphenylamino-3-cyano-[1,1′-biphenyl]-4-yl)ethynyl)-2,5-bis(2-ethylhexyloxy)-benzene (**2EHO-TPA-CNPE**).

CuI/Et$_3$N co-catalyst/base in THF affording the dibrominated intermediate **2EHO-Br-CNPE** in 71% yield. This reaction involved very selective Sonogashira cross-couplings to the iodo positions with a yield of 84% at each reaction site. The selectivity undoubtedly arises from the better reactivity of iodo as compared to bromo and the presence of electron-withdrawing cyano group *ortho* to the iodo substituent, both of which facilitates rate-determining oxidative addition step in the catalytic cycle.[47,48] In the final step, Suzuki cross-coupling reaction between triphenylamine pinacol boronic ester and **2EHO-Br-CNPE** was performed in the presence of Pd(PPh$_3$)$_4$ catalyst and Na$_2$CO$_3$ base in dimethoxyethane (DME), which yielded the target molecule **2EHO-TPA-CNPE** in 65% yield. Despite its large molecular weight (1071.39 amu), **2EHO-TPA-CNPE** was found to be quite soluble in common organic solvents such as chloroform and THF, as well as printing friendly solvents such as toluene and xylene. **2EHO-TPA-CNPE** was purified by column chromatography on silica gel using CH$_2$Cl$_2$: *n*-hexane (3 : 1, v/v) solvent mixture. The chemical structures and purities of the intermediate compounds and the final molecule were characterized with ^{1}H/^{13}C NMR spectroscopies (Fig. S2–S6, S8, and S9, ESI†), MALDI-TOF mass spectrometry (Fig. S7 and S10, ESI†), and elemental analysis.

Thermal properties

Thermal properties of the new molecule were studied by thermogravimetric analysis (TGA) and differential scanning calorimetry (DSC) (Fig. 3). The thermolysis onset temperature (T_{onset}, 5% weight loss) of 380 °C indicates an excellent thermal stability for the new molecule. In comparison to deep-blue emissive **2EHO-CNPE** (T_{onset} = 346 °C),[38] **2EHO-TPA-CNPE**'s increased thermal stability (ΔT_{onset} = +34 °C) against thermolysis is the result of terminal diphenylamino moieties introducing additional aryl units (6 extra phenyls per molecule) on the molecular backbone. The DSC characterization of the **2EHO-TPA-CNPE** solid, which was crystallized from the solvent removal after chromatography, shows a sharp endothermic peak at 195 °C (enthalpy of 38.89 J g^{-1}) corresponding to the melting point of the solid ($T_{m.p.}$ = 193–194 °C). Prior to the isotropic transition, two endothermic peaks at 155 °C (enthalpy of 49.56 J g^{-1}) and 164 °C (enthalpy of 39.12 J g^{-1}) were observed, which indicates the presence of mesophase(s) at temperatures higher than ~150 °C for this molecule.[49] The isotropic liquid phase of **2EHO-TPA-CNPE** was found to be transformed to a completely amorphous phase upon cooling since no crystallization peak was observed and the successive heating cycle yields only a glass transition (T_g) at 82 °C with no melting. The amorphous morphology of the **2EHO-TPA-CNPE** solid is consistent with those of previously reported arylamine terminated emissive and hole-transport small molecules.[44,50,51] Much higher melting temperature of **2EHO-TPA-CNPE** ($\Delta T_{m.p.}$ ~ 80 °C), in comparison to that of the deep-blue emissive **2EHO-CNPE** ($T_{m.p.}$ = 116–117 °C), reflects its extended molecular π-backbone with increased donor–acceptor characteristics.
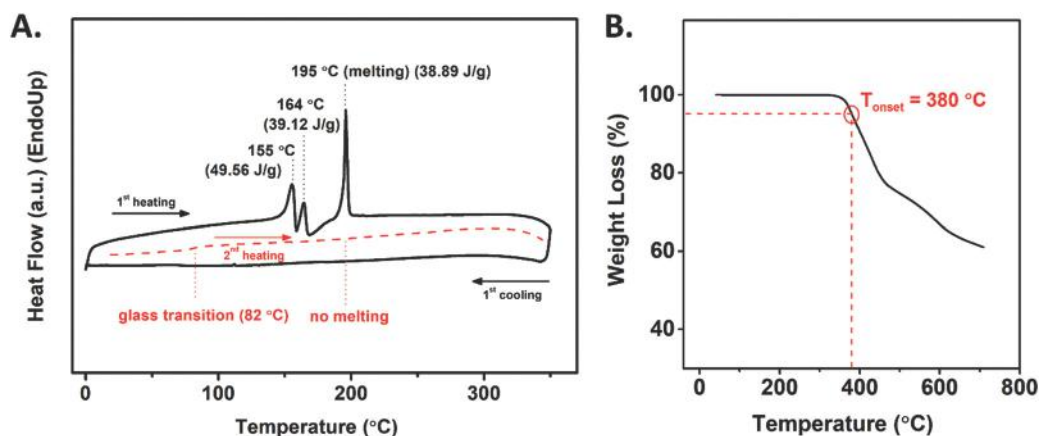

Fig. 3 Differential scanning calorimetry (DSC) measurement curves (A) and thermogravimetric analysis (TGA) curve (B) of **2EHO-TPA-CNPE** at a temperature ramp of 10 °C min^{-1} under N$_2$.

8052 | *J. Mater. Chem. C*, 2020, **8**, 8047–8060

This journal is © The Royal Society of Chemistry 2020

Photophysical/electrochemical properties and solvatochromic effects

Photophysical properties of the new molecule were studied by optical absorption, steady-state photoluminescence, and transient photoluminescence spectroscopies in different solutions with varied polarities (1×10^{-5} M, hexane → acetonitrile) and as thin-films. As depicted in Fig. 4A, **2EHO-TPA-CNPE** showed an absorption maximum (λ_{abs}^{max}) at 417 nm in dichloromethane solution that corresponds to π–π* ($S_0 \rightarrow S_1$) transition of the molecular backbone. The corresponding photoluminescence spectrum in dichloromethane solution displays a green fluorescence emission with a peak maximum (λ_{fl}^{max}) at 519 nm. The photoluminescence quantum efficiency measured by using the integrating-sphere method was found to be near unity ($\Phi_{PL} = 0.95$). This indicates a very efficient radiative $S_1 \rightarrow S_0$ electronic transition on the molecular backbone with minimal non-radiative losses. From the intersection of low-energy absorption (λ_{abs}^{0-0}) and high-energy fluorescence (λ_{fl}^{0-0}) spectral band edges, the optical band gap is measured as 2.68 eV, which is consistent with the TDDFT-calculated $S_0 \rightarrow S_1$ electronic transition (2.48 eV, HOMO → LUMO ($f = 2.32$), Fig. S1, ESI†).

Both absorption and fluorescence peaks, as well as the optical band gap, for the new molecule are found to be shifted significantly to lower energies ($\Delta(\lambda_{abs}^{max}) = +30$ nm, $\Delta(\lambda_{fl}^{max}) = +85$ nm, $\Delta E_g = -0.3$ eV) relative to the deep-blue emissive **2EHO-CNPE**.[38] These spectral changes are obviously the result of extended π-conjugation of the new molecule and increased donor–acceptor nature of the backbone. Going from solution to solid-state, slightly red-shifted absorption ($\Delta\lambda_{abs}^{max} = +19$ nm) profile was obtained (Fig. 4A) that most likely originates from intramolecular π-planarization formed in the solid-state. The solid-state (neat spin-coated thin-film) fluorescence spectrum of **2EHO-TPA-CNPE** has λ_{fl}^{max} at 518 nm showing almost no change from that in the dichloromethane solution. This indicates that the intermolecular interactions formed in the solid-state does not change the excitonic properties of the new molecule and the polarity created by the molecules itself in the solid-state (solid-state solvation effect)[30,52,53] is similar to that of the medium polarity solvent, dichloromethane. Because the thin-film fluorescence emission remains in the green spectral region showing a favorable full width at half-maximum (fwhm ∼ 70 nm), the desired green emitting OLEDs could be
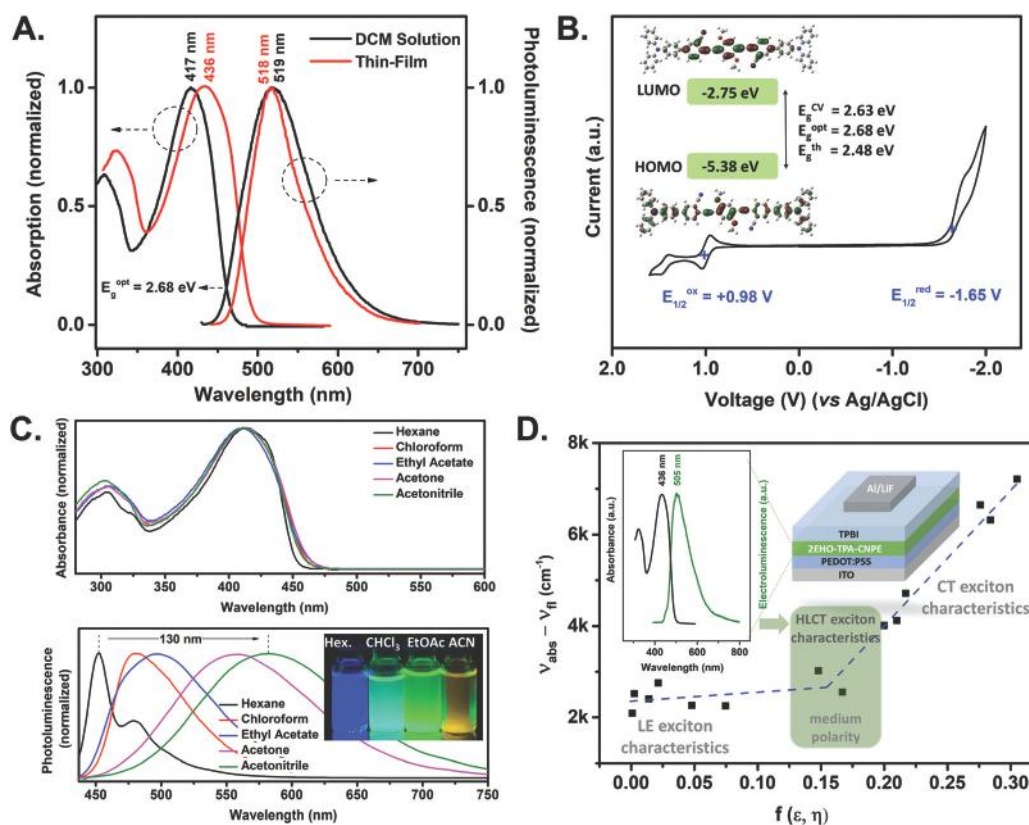

Fig. 4 (A) Optical absorption and photoluminescence spectra of **2EHO-TPA-CNPE** in dichloromethane (1.0×10^{-5} M) and as spin-coated neat thin-film on glass. (B) Cyclic voltammogram of **2EHO-TPA-CNPE** showing oxidation and reduction peaks in 0.1 M TBAPF₆/CH₂Cl₂ solution *vs.* Ag/AgCl (3.0 M NaCl) at a scan rate of 100 mV s⁻¹. Inset shows the experimental HOMO/LUMO energy levels, Frontier orbital topographies, and optical/electrochemical/theoretical band gaps. (C) Solvatochromic optical absorption and photoluminescence spectra of **2EHO-TPA-CNPE** in different solvents with increasing polarity (hexanes → acetonitrile). Inset shows the optical images of **2EHO-TPA-CNPE** solutions in different solvents under optical excitation. (D) Solvatochromic Lippert–Mataga model showing the fitted linear correlation ($\nu_{abs} - \nu_{fl}$ *vs.* $f(\varepsilon,n)$), and LE-dominated, CT-dominated, and HLCT excitonic regions. Inset shows the device architecture and solid-state absorption/electroluminescence profiles for **2EHO-TPA-CNPE**-based green emitting OLED device.

fabricated without needing a host matrix. The thin-film photoluminescence quantum efficiency was measured as 0.45 by using the integrating-sphere method. Electrochemical characterization reveals the coexistence of clear (quasi)reversible oxidation and reduction peaks in the same cyclic voltammetry scan at +0.98 V and −1.65 V (vs. Ag/AgCl), respectively (Fig. 4B). This reflects bipolar charge-transport nature of the new emissive molecule, which potentially would allow for efficient hole and electron injection/transport in the emissive layer. The LUMO and HOMO energies are estimated to be −2.75 eV and −5.38 eV, respectively. In agreement with the optical and theoretical band gap values, the electrochemical band gap (E_g^{CV}) is measured as 2.63 eV. As compared with deep-blue emissive **2EHO-CNPE**, LUMO of the new molecule remains almost the same (ΔE_{LUMO} = +0.04 eV) while HOMO considerably increases (ΔE_{HOMO} = +0.45 eV), which is very consistent with the DFT results (ΔE_{LUMO}th/ΔE_{HOMO}th = +0.07/+0.40 eV) and the corresponding orbital topographies (Fig. 2).

In order to explore the excited state characteristics, optical absorption and photoluminescence spectra of **2EHO-TPA-CNPE** were studied in fourteen different solvents with wide-ranging orientational polarizabilities ($f(\varepsilon,n)$). As shown in Fig. 4C and Fig. S11, S12 (ESI†), upon increasing solvent polarity (hexane ($f(\varepsilon,n)$ = 0.001) → acetonitrile ($f(\varepsilon,n)$ = 0.305)), although the absorption profiles remain almost the same, photoluminescence spectra exhibit extremely large bathochromic shifts of up to 130 nm. The complete data is provided on Table S2 (ESI†). This clearly suggests that while the ground state (S_0) of **2EHO-TPA-CNPE** is not of any CT character, the radiative excited state (S_1) possesses significant intramolecular CT character with a large excited state dipole moment. Interestingly, the spectral red shifts in the high polarity region (481 nm (chloroform) → 582 nm (acetonitrile), $\Delta f(\varepsilon,n)$ = 0.15) was found to be much more pronounced than that (452 nm (hexane) → 481 nm (chloroform), $\Delta f(\varepsilon,n)$ = 0.15) in the low polarity region. This clearly suggests that there are two different excited state behaviors in the low and high solvent polarity regions for **2EHO-TPA-CNPE** π-system. The excited state dipole moment (μ_e) of the S_1 state could be estimated from the slope of the Lippert–Mataga plot (Stokes shifts ($\nu_{abs} - \nu_{fl}$) against $f(\varepsilon,n)$) and using the DFT-calculated ground state dipole moment (see ESI† for details). As shown in Fig. 4D, two section linear fittings were obtained in the low and high solvent polarity regions giving two different excitonic characters. Based on the fitted line slopes, it is clear that S_1 shows LE-dominated excitonic character in the low-polarity region and CT-dominated excitonic character in the high-polarity region. The LE-dominated excited state character was evident in the vibrational fine structure of the photoluminescence spectra in this region. The emission peak intervals were found to be in the order of 0.17–0.20 eV ($\sim$1400–1600 cm^{-1}) corresponding to the vibrational frequencies of aromatic C=C bond stretches.[54,55] Going to high-polarity region, vibronic structure of the fluorescence spectrum completely disappears and significant emission band broadening was observed, surely reflecting the CT character dominance in the excited state. The fwhm becomes $\sim$135 nm in acetonitrile

while it is estimated to be as narrow as $\sim$35–40 nm in hexane. The slope of the curve in the high polarity region was found to be very large (slope $\approx$ 29 700 and R^2 = 0.97) yielding a μ_e of 35.3 D. Note that significantly large μ_e value of **2EHO-TPA-CNPE** is in the order of some of the highest excited state dipole moments predicted in the literature and it refers to a very strong CT character in the high polarity region.[33–35,56] The observed solvatochromic behavior for **2EHO-TPA-CNPE** reveals the presence of both LE and CT characteristics in the excited state, which tends to hybridize nonequivalently in the low- and high-polarity regions. However, (quasi)equivalent hybridization of LE and CT to generate a HLCT excited state character is very likely to occur in a medium polarity environment (f = 0.15–0.20) (Fig. 4D, green shaded area). The solution photoluminescence quantum efficiencies were measured as low as 0.25 and 0.15 in high-polarity acetone and acetonitrile solvents, respectively, as a result of strong CT character. Similarly, the quantum efficiency in the LE region was also found to be low (Φ_{PL} = 0.17 (in hexane)). The highest photoluminescence quantum efficiencies for the new molecule were measured in the HLCT region (Φ_{PL} = 0.94 (in chloroform), Φ_{PL} = 0.95 (in ethyl acetate), and Φ_{PL} = 0.95 (in dichloromethane)). When this solvatochromic behavior is compared with that of our previously developed deep-blue emissive molecule, μ_e's of **2EHO-CNPE** in both low- and high-polarity solvents are found to be undistinguishable yielding a single μ_e value of 8.4 D (R^2 = 0.96) (Fig. S13, ESI†). A good linearity retains across the whole solvent polarity region, which supports sufficiently hybridized (strong interstate coupling) LE and CT components in **2EHO-CNPE**'s HLCT excited state. The observed much stronger CT behavior in the excited state of the new molecule, as compared to **2EHO-CNPE**, is undoubtedly the result of extended π-conjugation with additional diphenylamino end units. Excitingly, the electroluminescence profile for **2EHO-TPA-CNPE**-based thin-film in OLED exhibits λ_{el}^{max} at 505 nm (Fig. 4D-inset) that corresponds to the medium solvent polarity HLCT region in the Lippert–Mataga plot. This indicates that the polar-environment created by the molecules itself in the neat thin-film (solid-state solvation effect)[30,52,53] could facilitate HLCT character in the excited state, which is highly beneficial to employ efficient radiative emission and triplet-to-singlet excitonic transition features at the same time during electroluminescence.

Electroluminescence properties and conventional/inverted/printed organic light-emitting diodes

Based on its good solubility in organic solvents, highly favorable photophysical and Frontier orbital (i.e., wave function topographies and energies) characteristics, and good thermal properties, **2EHO-TPA-CNPE** stands as a very promising candidate for solution-processed multilayered electroluminescent devices. In order to study the electroluminescence properties, OLED devices were first fabricated in a conventional device architecture of ITO/PEDOT:PSS(60 nm)/**2EHO-TPA-CNPE**(55 nm)/TPBI(40 nm)/LiF(0.8 nm)/Al(100 nm). Because **2EHO-TPA-CNPE** neat thin-film exhibits a favorable green fluorescence without a sign of undesirable aggregation-induced excimer emission, the

8054 | *J. Mater. Chem. C*, 2020, **8**, 8047–8060

This journal is © The Royal Society of Chemistry 2020

emissive layer in the current OLED device was prepared by spin-coating **2EHO-TPA-CNPE** solution (10 mg ml^{-1}) in chloroform without using a host matrix. The atomic force microscopy (AFM) characterization reveals that the new molecule forms a continuos amorphous morphology with highly interconnected granular domains ($\sim$50–100 nm in sizes) and a smooth organic surface (root mean square roughness <0.5 nm) on ITO/PEDOT:PSS (Fig. S14, ESI†). Energy level diagram of this device is shown in Fig. 5B, in which PEDOT:PTSS and LiF serve as hole- and electron-injecting layers, respectively; TPBI is used as electron-transport and hole-blocking layer. As shown in Fig. 5A and 6A, the device turns on at a voltage of 3.5 V (V_{on}, 1 cd m^{-2}), which is in the order of the band gap value of the emissive layer, and strong electroluminescence with a peak maximum at 505 nm (at 200 cd m^{-2}) was observed that corresponds to green emission with CIE 1976 (u', v') chromaticity coordinate of (0.10, 0.55). The electroluminescence profile of the new molecule coincides with the solid-state photoluminescence indicating that the radiative excitons formed under electrical bias are in the molecular S$_1$ state and excimer formation is effectively prevented. As shown in Fig. 5B, the (u', v') chromaticity coordinate of the new molecule occurs to be in the night vision imaging systems (NVIS) Green A region, which indicates that the new molecule holds great promise for use in NVIS compatible displays, especially for military and commercial avionics.[57,58] As shown in Fig. 6, **2EHO-TPA-CNPE**-based OLED device demonstrated good performance with a maximum current efficiency (CE$_{\text{max}}$) of 12.0 cd A^{-1}, a maximum power efficiency (PE$_{\text{max}}$) of 5.4 lm W^{-1}, and a maximum external quantum efficiency (EQE$_{\text{max}}$) of 4.5% (all values at $\sim$320 cd m^{-2}). The device maintains a chromaticity coordinate of (0.11, 0.55) and electroluminescence performance of CE = 10.8 cd A^{-1}, PE = 4.3 lm W^{-1}, and EQE = 4.0% under a high luminance value of

$\sim$1000 cd m^{-2}. On the basis of measured $\Phi_{\text{PL-neat film}}$ value of 0.45 and EQE$_{\text{max}}$ value of 4.5% (assuming $\eta_{\text{out}} \sim 0.2$ and $\gamma \sim 1$), it is evident that the radiative exciton yield ($\eta_{\text{r}} = \text{EQE}/(\gamma \times \Phi_{\text{PL}} \times \eta_{\text{out}})$) for the new molecule can reach as high as $\sim$50%.

Since such a strong solvatochromic behavior was seen in the photoluminescence of the new molecule that intensely tunes the excited state energy/dipole depending on the solvent polarity, we were interested in exploring whether a similar solid-state solvation effect could be observed on the electroluminescence properties of the OLED devices. For this purpose, OLEDs employing a **2EHO-TPA-CNPE**-based doped emissive layer (ITO/PEDOT:PSS(60 nm)/CBP:**2EHO-TPA-CNPE**(60 nm)/TPBI(40 nm)/LiF(0.8 nm)/Al(100 nm)) were fabricated with the same device architecture. The emissive layer was deposited by spin-coating chloroform solution of **2EHO-TPA-CNPE** (4.0 wt%) and 4,4′-bis(*N*-carbazolyl)-1,1′-biphenyl (CBP) (96.0 wt%) host matrix. CBP host was used based on its good charge-transport properties, proper Frontier orbital energies, and good spectral overlap between CBP's emission and **2EHO-TPA-CNPE**'s absorption bands (Fig. S15B and C, ESI†). Also, in contrast to the neat thin-film in which each **2EHO-TPA-CNPE** emissive molecule is neighboring similar molecules of strong donor–acceptor nature (high polarity), each emissive molecule in the doped thin-film is surrounded by relatively less polar CBP host molecules.[59] Consistent with the photoluminescence profile of this doped CBP:**2EHO-TPA-CNPE** thin-film (Fig. S15A, ESI†), the electroluminescence spectrum is found to show a sky-blue emission with a peak maximum at 475 nm (at 200 cd m^{-2}) and a (u', v') chromaticity coordinate of (0.09, 0.45) (Fig. S15, ESI†). Therefore, it is evident that the electroluminescence of **2EHO-TPA-CNPE** blue shifted as the polarity of the adjacent molecules decreased, which indicates the destabilization of the radiative S$_1$ state. This is in close agreement with the
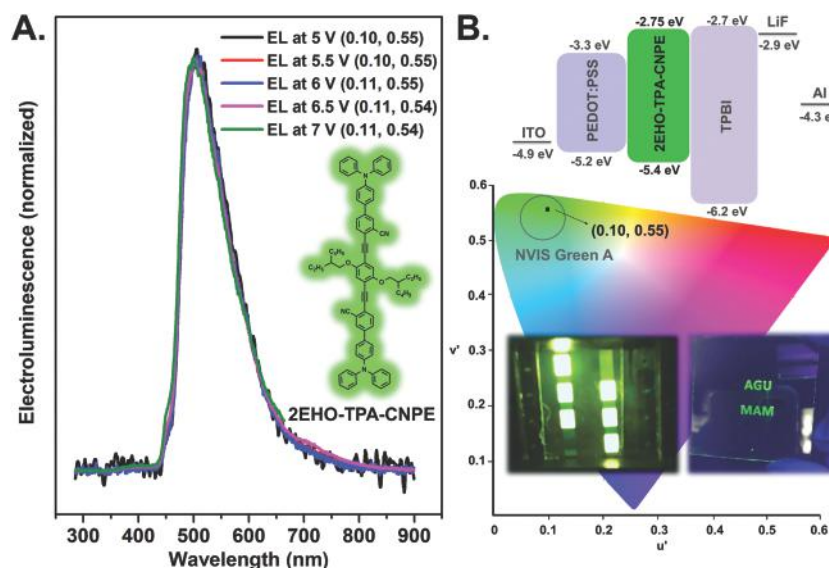

Fig. 5 (A) EL spectra and the corresponding CIE 1976 (u', v') chromaticity coordinates for **2EHO-TPA-CNPE**-based green emitting conventional OLED device (ITO/PEDOT:PSS(60 nm)/**2EHO-TPA-CNPE**(55 nm)/TPBI(40 nm)/LiF(0.8 nm)/Al(100 nm)) operated at different voltages. Inset shows the chemical structure of **2EHO-TPA-CNPE**. (B) Energy level diagram and CIE 1976 (u', v') chromaticity diagram showing NVIS Green A region and (u', v') coordinates of the green emitting OLED device at 200 cd m^{-2}. The insets show optical images of the OLEDs (9 mm^2 active area) during device operation and the letters (on a glass substrate) under UV light illumination based on ink-jet printed fluorescent **2EHO-TPA-CNPE** thin-films.
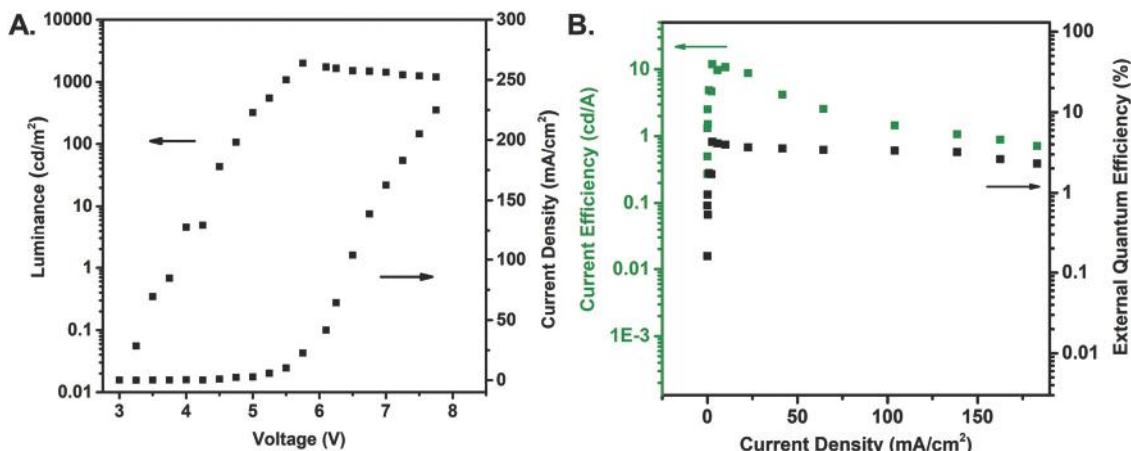
Fig. 6 Luminance–voltage–current density (A) and current efficiency–current density–external quantum efficiency (B) plots for **2EHO-TPA-CNPE**-based OLED device (ITO/PEDOT:PSS(60 nm)/**2EHO-TPA-CNPE**(55 nm)/TPBI(40 nm)/LiF(0.8 nm)/Al(100 nm)).

observed photoluminescence solvatochromic behavior, and the change in λ_{el}^{max} (505 nm → 475 nm) corresponds to a polarity change of $f(\varepsilon,n) = 0.21 \rightarrow 0.15$ in the HLCT excitonic region (Fig. 4D). Indeed, close inspection of the EL spectrum reveals that there is still a shoulder at ~505 nm, which might be due to residual presence of self-aggregated **2EHO-TPA-CNPE** molecules in the doped thin-film. The doped device exhibited an improved EQE_{max} of 5.5% with CE_{max} of 10.1 cd A^{-1} and PE_{max} of 4 lm W^{-1} (all values at 250 cd m^{-2}), which corresponds to $\eta_r = 59\%$ (using $\Phi_{\text{PL-doped film in CBP}} = 0.47$) (Fig. S16, ESI†). The η_r value for the doped CBP:**2EHO-TPA-CNPE** thin-film is ~9% higher than that of the neat **2EHO-TPA-CNPE** thin-film. Therefore, it is clear that the solid-state solvation effect does not only change the exciton energy level but also affect the yield of radiative exciton formation process.[60] Similar effects of host matrix polarity on RISC efficiency during molecular electroluminescence have been observed in previous studies.[30,61,62] Therefore, it is very likely that solid-state solvation effect for **2EHO-TPA-CNPE** could be finely tuned by using different host matrices to expand the scope of excitonic states (LE vs. HLCT vs. CT) for various optoelectronic applications.

In order to further explore the industrial relevance of the new molecule for organic optoelectronics, additional OLED devices were fabricated by ink-jet printing the emissive layer and by fabricating an inverted architecture. Although these devices are not fully optimized and show somewhat lower performances than conventional spin-coated devices, they are significant to demonstrate that **2EHO-TPA-CNPE** could potentially offer key manufacturing advantages. The high precision deposition of OLED materials by ink-jet printing is of great technological importance for making cost-effective flexible displays, because it could significantly reduce material waste and process complexity (less number of fabrication/lithographic steps).[63] However, the formulation of OLED materials into non-chlorinated printable inks is not straightforward; a delicate balance between molecular weight/size, solubility, solvent boiling point, viscosity, and surface tension is required for favorable printing and film drying processes to yield an efficient electroluminescent thin-film.[64] Initially, as a proof of

concept, shapes in letter characters, comprised of fluorescent **2EHO-TPA-CNPE**-based thin-film, were deposited onto a glass substrate via ink-jet printing (PIXDRO LP50) (Fig. 5B). In this process, jettable formulation of the new molecule was prepared in 1 mg ml^{-1} concentration in o-xylene:3-phenoxytoluene (50:50 v/v%) solvent mixture (viscosity = 2.1 mPa s at 22 °C). This non-chlorinated high boiling-low boiling solvent mixture was selected based on preliminary drop-casting experiments for an efficient printing process and to overcome any ring formation.[65] Proper droplet generation was achieved using print head KM512 at a voltage of 14 V and pulse width of 5 μs. The corresponding OLED devices were fabricated in a conventional device architecture (ITO/PEDOT:PSS(60 nm)/**2EHO-TPA-CNPE**(50 nm/ink-jet printed)/TPBI(40 nm)/LiF(0.8 nm)/Al(100 nm)), in which the emissive layer is ink-jet printed as a non-doped thin-film. The maximum current efficiency of this unoptimized printed device was 2.4 cd A^{-1} (at 250 cd m^{-2}) and the maximum luminance (L_{max}) was 550 cd m^{-2} ((u', v') = (0.16, 0.55)) (Fig. S17, ESI†). These results show that **2EHO-TPA-CNPE** has favorable molecular properties (structural size/solubility and photo-/electro-luminescence) making itself a promising material for the development of ink-jet printed display technologies. On the other hand, inverted OLED architecture of ITO/TNC(50 nm)/**2EHO-TPA-CNPE**(55 nm)/TPD(50 nm)/V$_2$O$_5$(15 nm)/Al(100 nm) was also studied with the new molecule. Inverted OLEDs with bottom cathode electrode are highly desirable for mass production of large area active-matrix displays as they can be easily integrated to the drain electrode of n-channel TFT backplane.[66] They also have higher stabilities resulting from the fact that water-/oxygen-sensitive electron-injecting layer remains under the emissive organic layer and metal oxides are used instead PEDOT:PSS.[66–68] Since electron-injecting layer plays a critical role in the performance of inverted OLEDs, a ternary nano-composite (TNC) of zinc oxide/polyethyleneimine/1,3,5-tris(N-phenylbenzimidazol-2-yl)-benzene (ZnO:PEI:TPBI) was used combining electron-injecting/-transport and hole-blocking characteristics.[43] In this inverted structure, Al (anode) and ITO (cathode) are used as electrodes while N,N'-bis(3-methylphenyl)-N,N'-diphenylbenzidine (TPD) and

8056 | J. Mater. Chem. C, 2020, **8**, 8047–8060

This journal is © The Royal Society of Chemistry 2020

V_2O_5 serve as hole-transport/electron-blocking and hole-injecting layers, respectively. The emissive **2EHO-TPA-CNPE**-based thin-film was deposited *via* spin-coating. The inverted device demonstrated a good performance with CE_{max} value of 6.1 cd A^{-1} (at 1250 cd m^{-2}) and L_{max} value of 3600 cd m^{-2} ((u', v') = (0.18, 0.55)) (Fig. S18, ESI†).

The photophysical properties of the new molecular π-system are further studied *via* TDDFT calculations (B3LYP/6-311G** level of theory), and time resolved and comparative (ambient *vs.* nitrogen atmosphere) photoluminescence spectroscopies. On the basis of the EQEs achieved, the radiative singlet exciton yields for **2EHO-CNPE-TPA**-based OLEDs ($\eta_r \sim$ 50–59%) exceed the spin-statistical limit of 25% for singlet exciton. Therefore, in agreement with our previously reported **2EHO-CNPE** molecule, triplet-to-singlet excited state conversions *via* RISC are likely to be effective during the electroluminescence process of the new molecule. To this end, TADF process is predicted to be energetically inefficient as the energy gap between S_1 and T_1 states ($\Delta E_{S_1-T_1}$ = 0.64 eV) is much larger than that required for TADF-based molecular electronic structures (typically $\Delta E_{S_1-T_1} \leq$ 100 meV).[18,69] However, as shown in Fig. 7A and C, hot-exciton channels employing RISC's from high-lying triplet excited states to the singlet excited state ($T_2 \to S_1$ and $T_3 \to S_1$) are identified to be quite favorable both from an energetic ($\Delta E_{S_1-T_2}$ =

0.11 eV and $\Delta E_{S_1-T_3}$ = 0.04 eV) and wave function characteristics standpoints. As clearly seen in the NTO wave functions (Fig. 7C and Table S3, ESI†), energetically close excited states S_1, T_2 and T_3 exhibit a good balance of spatial separation (CT) and orbital overlap (LE) along the molecular π-backbone. The coexistence of LE and CT characteristics (HLCT behavior) in the excited states is crucial to simultaneous realization of triplet-to-singlet excitonic conversions and $S_1 \to S_0$ radiative transition during electroluminescence. However, as compared with **2EHO-CNPE**, the CT character of the new molecule is found to be more pronounced. The NTO analysis shows significant wave function contributions from diphenylamino donor end units (D') for the hole NTOs, whereas the particle NTOs are found to be delocalized only on the central part (A–π–D–π–A). The increased CT characteristics of the excited states in the new molecule show a good agreement with the observed strong PL solvatochromic behavior (*vide supra*). As a result of extending π-conjugation, the energetic separations between the excited states of the same multiplicity become smaller in **2EHO-TPA-CNPE**. According to energy gap law, having a large $\Delta E_{T_2-T_1}$ is particularly important for efficient hot-exciton channel formation by minimizing undesired $T_2 \to T_1$ internal conversion ($k_{RISC} \gg k_{IC}$).[21,35] In the new molecule, although the $\Delta E_{S_1-T_2/T_3}$ is very similar to those of **2EHO-CNPE**, the energy difference
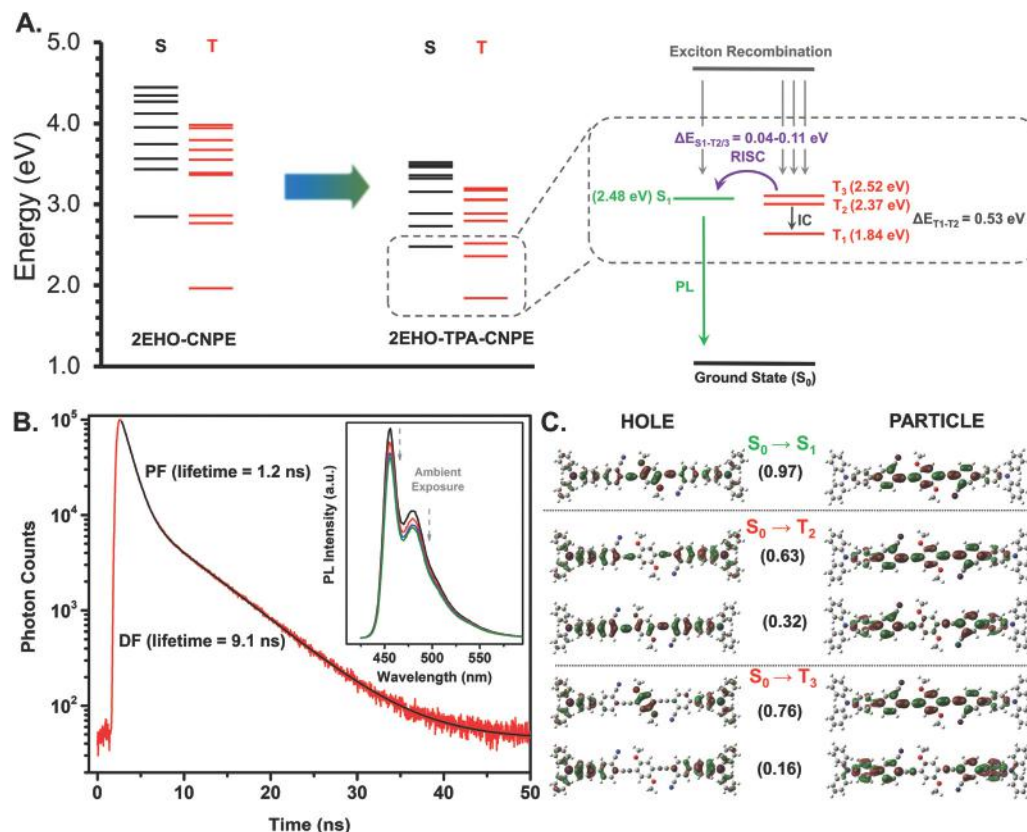

Fig. 7 (A) Energy levels of the first ten singlet/triplet excited states for our previously reported deep-blue emissive molecule **2EHO-CNPE** and the new green emissive molecule **2EHO-TPA-CNPE** calculated with TDDFT in S_0 geometry, and the proposed exciton decay processes (RISC, reverse intersystem crossing; IC, internal conversion; EL, electroluminescence). (B) The transient photoluminescence decay profile measured at 469 nm for **2EHO-TPA-CNPE** solution in hexane (10^{-5} M) under nitrogen atmosphere upon excitation at 375 nm and the corresponding lifetimes for prompt (PF) and delayed fluorescence (DF). The inset shows the gradual decrease in PL intensity when the same solution is exposed to ambient atmosphere. (C) Natural transition orbitals (NTOs) for **2EHO-CNPE-TPA**'s S_1, T_2 and T_3 excited states calculated with TDDFT. The coefficients of each hole–particle pair are given in parentheses.

between T_2 and T_1 excited states was found to be lower than that of **2EHO-CNPE** ($\Delta E_{T_1-T_2}$ = 0.53 eV < 0.81 eV), which partially explains the observed lower radiative exciton yield (η_r = 70% → 50–59%). At this point, we speculate that hot-exciton RISCs are likely to be more efficient with short π-conjugated systems since they usually tend to have wider T_1–T_2 separation to prevent undesired triplet ($T_2 \rightarrow T_1$) internal conversion. Indeed, consistent with this thought, the highest performing hot-exciton molecules reported in the literature are typically wide band gap (deep)-blue emissive π-systems.[33,38,70] We also note that while hot-exciton channels of $T_{2/3} \rightarrow S_1$ are very favorable to take place for the new molecule since these states are expected to have relatively higher population densities among all excited states, higher-energy hot-exciton channels (T_m ($m \geq 4$) → S_n ($n \geq 2$)) could not be excepted for radiative singlet exciton formation.[71,72] Indeed, our calculations with spin–orbit couplings indicate that triplet-to-singlet conversions could be favorable between these high-lying excited states when their energies match (Table S4 and Fig. S19, ESI†). The excited state properties of the new molecule were further studied *via* time-resolved photoluminescence decay measurements and comparative (ambient *vs.* nitrogen atmosphere) photoluminescence spectroscopy. The PL decay profile of the new molecule in nonpolar hexane solution was recorded under nitrogen atmosphere at the fluorescence maximum (λ_{exc} = 375 nm and 200 ps pulse width) by the time-correlated single photon counting method. As shown in Fig. 7B, double exponential decay profile was obtained showing first a prompt decay with a lifetime of 1.16 ns ($\sim$90% contribution) and then a delayed component with a relatively longer lifetime of 9.14 ns ($\sim$10% contribution). Note that, as expected, TADF mechanism-based fluorescence delays on a microsecond (μs) timescale were not observed. The prompt decay is identified as the direct $S_1 \rightarrow S_0$ electronic transition (fluorescence) originating from the photoexcited S_1 states. The longer lifetime component could be attributed to delayed $S_1 \rightarrow S_0$ fluorescence occurring through (R)ISCs between energetically matching S_1 and T_2/T_3 states because the PL spectrum of this delayed component is identical to that of the prompt fluorescence. To the best of our knowledge, this is one of the very few examples in the hot-exciton literature that high-energy RISC-related delayed fluorescence is directly observed in a PL decay profile without using a triplet sensitizer. Recently in the literature, Ma *et al.* reported similar lifetime scales for high-energy RISC processes ($\sim$14–20 ns) by employing a triplet sensitization technique.[22] A gradual decrease was observed in the PL intensity when the nitrogen-flushed solution was exposed to ambient atmosphere (Fig. 7B-inset), which further warrants that high-lying triplet state(s) are populated during the luminescence process, and they are somewhat quenched by triplet oxygen upon exposure to ambient atmosphere.[15,73,74]

Conclusions

In summary, a new highly soluble rod-shaped oligo(*p*-phenyleneethynylene) molecule, 1,4-bis((4′-diphenylamino-3-cyano-[1,1′-biphenyl]-4-yl)ethynyl)-2,5-bis(2-ethylhexyloxy)benzene (**2EHO-TPA-CNPE**) has

been designed, synthesized, and characterized. The thermal, photophysical, electrochemical, and electroluminescence properties have been studied in detail. Highly efficient green luminescence was achieved with the new molecule yielding high photoluminescence quantum efficiencies (Φ_{PL}'s) of 0.95 (solution) and 0.45 (neat thin-film), and high ($\gg$25%) radiative exciton yields of η_r = 50–59% in electroluminescence. A strong solvatochromic behavior was observed in photoluminescence as evident in significant changes in the excited state energies ($\Delta\lambda_{fl}^{max}$ = +130 nm) and characteristics (LE → HLCT → CT) upon polarity increase. The electroluminescence of the emissive thin-film in OLEDs was also found to be governed by the polarity of the surrounding molecules (solid-state solvation effect) that tunes emission profile and radiative exciton yield. The (non-)doped thin-films of the new molecule facilitate HLCT character in the excited state, which is very crucial to realize both radiative $S_1 \rightarrow S_0$ emission and triplet-to-singlet excitonic transitions ($T_{2/3} \rightarrow S_1$) in electroluminescence as supported by TDDFT calculations. Conventional OLED employing spin-coated non-doped **2EHO-TPA-CNPE** thin-film showed maximum current efficiency (CE_{max}) of 12.0 cd A^{-1}, a maximum power efficiency (PE_{max}) of 5.4 lm W^{-1}, and a maximum external quantum efficiency (EQE_{max}) of 4.5% with an emission profile in the night vision imaging systems (NVIS) Green A region. OLEDs fabricated by doping the new molecule in CBP host matrix showed a sky-blue emission with improved EQE_{max} of 5.5%. Industrially more relevant OLED devices were also fabricated by ink-jet printing the emissive layer and by fabricating an inverted architecture, which showed reputable device performances of 2.4 cd A^{-1} and 6.1 cd A^{-1}, respectively. A ns-scale delayed fluorescence ($\sim$10 ns) due to high-lying (R)ISCs was confirmed in the PL decay profile following a prompt fluorescence decay ($\sim$1 ns). To the best of our knowledge, this result is one of the very few examples in the hot-exciton literature that high-lying RISC-related delayed fluorescence could directly be observed in a PL decay profile without using a triplet sensitizer. The findings presented in this study show that oligo-(*p*-phenyleneethynylene) π-framework with proper functionalities and substituents could be an important molecular family for high efficiency solution-processed OLED devices with a wide-color-gamut. Especially, the printing ability of the new molecule is very significant. With these new results, the crucial structure–photophysical property–electroluminescence relationships for oligo-(*p*-phenyleneethynylene)s are now better established to lead future hot-exciton material designs. However, one should note that the electronic structure for a newly designed molecule needs to be carefully tuned with regards to excited state energetic separations and wave function characteristics to realize the highest possible radiative exciton yield. The fact that the new molecule shows a wide range of excitonic characteristics (LE → HLCT → CT) tunable by medium polarity, both in solution and solid-state, could open up new opportunities for optoelectronic and molecular sensing applications.

Conflicts of interest

There are no conflicts to declare.

8058 | *J. Mater. Chem. C*, 2020, **8**, 8047–8060

This journal is © The Royal Society of Chemistry 2020

Acknowledgements

References

1 Q. Wei, N. Fei, A. Islam, T. Lei, L. Hong, R. Peng, X. Fan, L. Chen, P. Gao and Z. Ge, *Adv. Opt. Mater.*, 2018, **6**, 1800512.

2 M. Ozdemir, D. Choi, G. Kwon, Y. Zorlu, H. Kim, M.-G. Kim, S. Seo, U. Sen, M. Citir, C. Kim and H. Usta, *RSC Adv.*, 2016, **6**, 212–226.

3 R. Ozdemir, S. Park, İ. Deneme, Y. Park, Y. Zorlu, H. A. Alidagi, K. Harmandar, C. Kim and H. Usta, *Org. Chem. Front.*, 2018, **5**, 2912–2924.

4 S.-H. Lee, B. Lim, M. Pei, H. Yang and Y.-Y. Noh, *J. Mater. Chem. C*, 2018, **6**, 7604–7611.

5 Y. Liu, L. Zhang, H. Lee, H.-W. Wang, A. Santala, F. Liu, Y. Diao, A. L. Briseno and T. P. Russell, *Adv. Energy Mater.*, 2015, **5**, 1500195.

6 R. Capelli, S. Toffanin, G. Generali, H. Usta, A. Facchetti and M. Muccini, *Nat. Mater.*, 2010, **9**, 496–503.

7 D. Ho, R. Ozdemir, H. Kim, T. Earmme, H. Usta and C. Kim, *ChemPlusChem*, 2019, **84**, 18–37.

8 D. Khim, K.-J. Baeg, J. Kim, M. Kang, S.-H. Lee, Z. Chen, A. Facchetti, D.-Y. Kim and Y.-Y. Noh, *ACS Appl. Mater. Interfaces*, 2013, **5**, 10745–10752.

9 K.-J. Baeg, M. Caironi and Y.-Y. Noh, *Adv. Mater.*, 2013, **25**, 4210–4244.

10 J. Park, C. Lee, J. Jung, H. Kang, K.-H. Kim, B. Ma and B. J. Kim, *Adv. Funct. Mater.*, 2014, **24**, 7588–7596.

11 A. Sharenko, N. D. Treat, J. A. Love, M. F. Toney, N. Stingelin and T.-Q. Nguyen, *J. Mater. Chem. A*, 2014, **2**, 15717–15721.

12 M. A. Baldo, D. F. O'Brien, Y. You, A. Shoustikov, S. Sibley, M. E. Thompson and S. R. Forrest, *Nature*, 1998, **395**, 151–154.

13 M. A. Baldo, D. F. O'Brien, M. E. Thompson and S. R. Forrest, *Phys. Rev. B: Condens. Matter Mater. Phys.*, 1999, **60**, 14422–14428.

14 C. Cho, H. Kang, S.-W. Baek, T. Kim, C. Lee, B. J. Kim and J.-Y. Lee, *ACS Appl. Mater. Interfaces*, 2016, **8**, 27911–27919.

15 Z. Yang, Z. Mao, Z. Xie, Y. Zhang, S. Liu, J. Zhao, J. Xu, Z. Chi and M. P. Aldred, *Chem. Soc. Rev.*, 2017, **46**, 915–1016.

16 D. Y. Kondakov, *Philos. Trans. R. Soc., A*, 2015, **373**, 20140321.

17 D. Y. Kondakov, T. D. Pawlik, T. K. Hatwar and J. P. Spindler, *J. Appl. Phys.*, 2009, **106**, 124510.

18 H. Uoyama, K. Goushi, K. Shizu, H. Nomura and C. Adachi, *Nature*, 2012, **492**, 234–238.

19 Y. Yu, L. Ma, Z. Feng, B. Liu, H. Zhou, H. Qin, H. Li, J. Song, G. Zhou and Z. Wu, *J. Mater. Chem. C*, 2019, **7**, 5604–5614.

20 T. Komino, H. Nomura, T. Koyanagi and C. Adachi, *Chem. Mater.*, 2013, **25**, 3038–3047.

21 N. J. Turro, *Modern Molecular Photochemistry*, University Science Books, Sausalito, Ca, 1991.

22 Y. Xu, X. Liang, X. Zhou, P. Yuan, J. Zhou, C. Wang, B. Li, D. Hu, X. Qiao, X. Jiang, L. Liu, S. Su, D. Ma and Y. Ma, *Adv. Mater.*, 2019, **31**, 1807388.

23 D. Hu, L. Yao, B. Yang and Y. Ma, *Philos. Trans. R. Soc., A*, 2015, **373**, 20140318.

24 W. Li, Y. Pan, R. Xiao, Q. Peng, S. Zhang, D. Ma, F. Li, F. Shen, Y. Wang, B. Yang and Y. Ma, *Adv. Funct. Mater.*, 2014, **24**, 1609–1614.

25 M. Segal, M. Singh, K. Rivoire, S. Difley, T. Van Voorhis and M. A. Baldo, *Nat. Mater.*, 2007, **6**, 374–378.

26 S. Difley, D. Beljonne and T. Van Voorhis, *J. Am. Chem. Soc.*, 2008, **130**, 3420–3427.

27 A. Kadashchuk, A. Vakhnin, I. Blonski, D. Beljonne, Z. Shuai, J. L. Brédas, V. I. Arkhipov, P. Heremans, E. V. Emelianova and H. Bässler, *Phys. Rev. Lett.*, 2004, **93**, 066803.

28 W. Li, Y. Pan, L. Yao, H. Liu, S. Zhang, C. Wang, F. Shen, P. Lu, B. Yang and Y. Ma, *Adv. Opt. Mater.*, 2014, **2**, 892–901.

29 C. Wang, X. Li, Y. Pan, S. Zhang, L. Yao, Q. Bai, W. Li, P. Lu, B. Yang, S. Su and Y. Ma, *ACS Appl. Mater. Interfaces*, 2016, **8**, 3041–3049.

30 W. Z. Yuan, X. Bin, G. Chen, Z. He, J. Liu, H. Ma, Q. Peng, B. Wei, Y. Gong, Y. Lu, G. He and Y. Zhang, *Adv. Opt. Mater.*, 2017, **5**, 1700466.

31 C. Fu, S. Luo, Z. Li, X. Ai, Z. Pang, C. Li, K. Chen, L. Zhou, F. Li, Y. Huang and Z. Lu, *Chem. Commun.*, 2019, **55**, 6317–6320.

32 W. Li, D. Liu, F. Shen, D. Ma, Z. Wang, T. Feng, Y. Xu, B. Yang and Y. Ma, *Adv. Funct. Mater.*, 2012, **22**, 2797–2803.

33 S. Zhang, L. Yao, Q. Peng, W. Li, Y. Pan, R. Xiao, Y. Gao, C. Gu, Z. Wang, P. Lu, F. Li, S. Su, B. Yang and Y. Ma, *Adv. Funct. Mater.*, 2015, **25**, 1755–1762.

34 J. Jayabharathi, S. Panimozhi and V. Thanikachalam, *RSC Adv.*, 2018, **8**, 37324–37338.

35 L. Yao, S. Zhang, R. Wang, W. Li, F. Shen, B. Yang and Y. Ma, *Angew. Chem., Int. Ed.*, 2014, **53**, 2119–2123.

36 H. Zhang, J. Zeng, W. Luo, H. Wu, C. Zeng, K. Zhang, W. Feng, Z. Wang, Z. Zhao and B. Z. Tang, *J. Mater. Chem. C*, 2019, **7**, 6359–6368.

37 Y. Gao, S. Zhang, Y. Pan, L. Yao, H. Liu, Y. Guo, Q. Gu, B. Yang and Y. Ma, *Phys. Chem. Chem. Phys.*, 2016, **18**, 24176–24184.

38 H. Usta, D. Alimli, R. Ozdemir, S. Dabak, Y. Zorlu, F. Alkan, E. Tekin and A. Can, *ACS Appl. Mater. Interfaces*, 2019, **11**, 44474–44486.

39 M. M. J. Frisch, G. W. Trucks, H. B. Schlegel, G. E. Scuseria, H. A. Robb, J. R. Cheeseman, G. Scalmani, V. Barone, B. Mennucci, G. A. Petersson, J. L. Nakatsuji, M. Caricato, X. Li, H. P. Hratchian, A. F. Izmaylov, J. Bloino, G. Zheng, T. Sonnenberg, M. Hada, M. Ehara, K. Toyota, R. Fukuda, J. Hasegawa, M. Ishida, F. Nakajima, Y. Honda, O. Kitao, H. Nakai, T. Vreven, J. A. Montgomery, Jr., J. E. Peralta, R. Ogliaro, M. Bearpark, J. J. Heyd, E. Brothers, K. N. Kudin, V. N. Staroverov, J. Kobayashi, J. Normand, K. Raghavachari, A. Rendell, J. C. Burant, S. S. Iyengar, C. Tomasi, M. Cossi, N. Rega, J. M. Millam, M. Klene, J. E. Knox, J. B. Cross,

This journal is © The Royal Society of Chemistry 2020

J. Mater. Chem. C, 2020, **8**, 8047–8060 | **8059**

V. Bakken, C. Adamo, J. Jaramillo, R. Gomperts, R. E. Stratmann, O. Yazyev, A. J. Austin, R. Cammi, P. Pomelli, J. W. Ochterski, R. L. Martin, K. Morokuma, V. G. Zakrzewski, G. A. Voth, J. V. Salvador, J. J. Dannenberg, S. Dapprich, A. D. Daniels, Ö. Farkas, J. B. Foresman, J. V. Ortiz, J. Cioslowski and D. J. Fox, *Gaussian 09, Revision C.01*, Gaussian, Inc., Wallingford, CT, USA, 2010.

40 ADF2019, SCM, Theoretical Chem. Vrije Univ. Amsterdam, Netherlands, http://www.scm.com.

41 G. te Velde, F. M. Bickelhaupt, E. J. Baerends, C. Fonseca Guerra, S. J. A. van Gisbergen, J. G. Snijders and T. Ziegler, *J. Comput. Chem.*, 2001, **22**, 931–967.

42 C. Fonseca Guerra, J. G. Snijders, G. Velde and E. J. Baerends, *Theor. Chem. Acc.*, 1998, **99**, 391–403.

43 R. Kaçar, S. P. Mucur, F. Yıldız, S. Dabak and E. Tekin, *Appl. Phys. Lett.*, 2018, **112**, 163302.

44 N. Tamoto, C. Adachi and K. Nagai, *Chem. Mater.*, 1997, **9**, 1077–1085.

45 S.-Y. Ku, L.-C. Chi, W.-Y. Hung, S.-W. Yang, T.-C. Tsai, K.-T. Wong, Y.-H. Chen and C.-I. Wu, *J. Mater. Chem.*, 2009, **19**, 773–780.

46 C.-G. Zhen, Z.-K. Chen, Q.-D. Liu, Y.-F. Dai, R. Y. C. Shin, S.-Y. Chang and J. Kieffer, *Adv. Mater.*, 2009, **21**, 2425–2429.

47 N. Miyaura and A. Suzuki, *Chem. Rev.*, 1995, **95**, 2457–2483.

48 R. Chinchilla and C. Nájera, *Chem. Soc. Rev.*, 2011, **40**, 5084–5121.

49 R. Ozdemir, D. Choi, M. Ozdemir, H. Kim, S. T. Kostakoğlu, M. Erkartal, H. Kim, C. Kim and H. Usta, *ChemPhysChem*, 2017, **18**, 850–861.

50 P. Kochapradist, N. Prachumrak, R. Tarsang, T. Keawin, S. Jungsuttiwong, T. Sudyoadsuk and V. Promarak, *Tetrahedron Lett.*, 2013, **54**, 3683–3687.

51 Z. H. Li, M. S. Wong, H. Fukutani and Y. Tao, *Chem. Mater.*, 2005, **17**, 5032–5040.

52 C. F. Madigan and V. Bulović, *Phys. Rev. Lett.*, 2003, **91**, 247403.

53 V. Bulović, R. Deshpande, M. Thompson and S. Forrest, *Chem. Phys. Lett.*, 1999, **308**, 317–322.

54 H. Usta, C. Risko, Z. Wang, H. Huang, M. K. Deliomeroglu, A. Zhukhovitskiy, A. Facchetti and T. J. Marks, *J. Am. Chem. Soc.*, 2009, **131**, 5586–5608.

55 A. Yassar, G. Horowitz, P. Valat, V. Wintgens, M. Hmyene, F. Deloffre, P. Srivastava, P. Lang and F. Garnier, *J. Phys. Chem.*, 1995, **99**, 9155–9159.

56 C. Deng, S. Zheng, D. Wang, J. Yang, Y. Yue, M. Li, Y. Zhou, S. Niu, L. Tao, T. Tsuboi and Q. Zhang, *J. Phys. Chem. C*, 2019, **123**, 29875–29883.

57 M. Nodari, F. Zaraga and R. Grassetti, *J. Soc. Inf. Disp.*, 2008, **16**, 343–349.

58 F. Zheng, X. Shi, K. Huan, Y. Li, L. Liu, L. Xu and G. Liu, *2012 International Conference on Optoelectronics and Microelectronics*, IEEE, 2012, pp. 157–161.

59 J.-H. Jou, Y.-P. Lin, M.-F. Hsu, M.-H. Wu and P. Lu, *Appl. Phys. Lett.*, 2008, **92**, 193314.

60 S. Ahn, J. N. Kim and Y. C. Kim, *Curr. Appl. Phys.*, 2015, **15**, S42–S47.

61 P. L. dos Santos, J. S. Ward, M. R. Bryce and A. P. Monkman, *J. Phys. Chem. Lett.*, 2016, **7**, 3341–3346.

62 T. Chatterjee and K.-T. Wong, *Adv. Opt. Mater.*, 2019, **7**, 1800565.

63 E. Tekin, P. J. Smith and U. S. Schubert, *Soft Matter*, 2008, **4**, 703–713.

64 T. Lin, X. Sun, Y. Hu, W. Mu, Y. Sun, D. Zhang, Z. Su, B. Chu and Z. Cui, *Sci. Rep.*, 2019, **9**, 6845.

65 E. Tekin, B.-J. de Gans and U. S. Schubert, *J. Mater. Chem.*, 2004, **14**, 2627–2632.

66 R. Kaçar, S. P. Mucur, F. Yıldız, S. Dabak and E. Tekin, *Nanotechnology*, 2017, **28**, 245204.

67 H. Fukagawa, K. Morii, M. Hasegawa, Y. Arimoto, T. Kamada, T. Shimizu and T. Yamamoto, *Appl. Phys. Express*, 2014, **7**, 082104.

68 J. Meyer, S. Hamwi, M. Kröger, W. Kowalsky, T. Riedl and A. Kahn, *Adv. Mater.*, 2012, **24**, 5408–5427.

69 P. K. Samanta, D. Kim, V. Coropceanu and J.-L. Brédas, *J. Am. Chem. Soc.*, 2017, **139**, 4042–4051.

70 S. Zhang, W. Li, L. Yao, Y. Pan, F. Shen, R. Xiao, B. Yang and Y. Ma, *Chem. Commun.*, 2013, **49**, 11302–11304.

71 R. Chen, Y. Tang, Y. Wan, T. Chen, C. Zheng, Y. Qi, Y. Cheng and W. Huang, *Sci. Rep.*, 2017, **7**, 6225.

72 S. Hirata, Y. Sakai, K. Masui, H. Tanaka, S. Y. Lee, H. Nomura, N. Nakamura, M. Yasumatsu, H. Nakanotani, Q. Zhang, K. Shizu, H. Miyazaki and C. Adachi, *Nat. Mater.*, 2015, **14**, 330–336.

73 N. Jürgensen, A. Kretzschmar, S. Höfle, J. Freudenberg, U. H. F. Bunz and G. Hernandez-Sosa, *Chem. Mater.*, 2017, **29**, 9154–9161.

74 A. Endo, K. Sato, K. Yoshimura, T. Kai, A. Kawada, H. Miyazaki and C. Adachi, *Appl. Phys. Lett.*, 2011, **98**, 083302.